Available online at www.sciencedirect.com
SCIENCE DIRECT
Cryogenics 46 (2006) 541–555
Cryogenics
www.elsevier.com/locate/cryogenics

A review of thermal-hydraulic issues in ITER cable-in-conduit conductors

R. Zanino *, L. Savoldi Richard

Dipartimento di Energetica, Politecnico, I-10129 Torino, Italy

Abstract

Problems related to cable-in-conduit conductors (CICC) are intrinsically multi-physics involving coupled electro-magnetic/mechanical/thermal-hydraulic fields. Here we concentrate on the thermal-hydraulic issues because, although the CICC was first proposed for the low-T_C superconducting coils of the International Thermonuclear Experimental Reactor (ITER) many years ago, CICC thermal-hydraulics alone is less understood than could be expected. Some of the difficulties are due to the multi-channel nature of the ITER CICC, where strands containing the superconducting filaments are twisted in multi-stage sub-bundles (petals) delimited by wrappings and concentrated in an annular (porous-medium like) region, while a central channel, delimited by a spiral, provides lower hydraulic impedance and pressure relief to the flow of the supercritical helium coolant. Other difficulties are related to the multi-scale nature of this problem, with length scales relevant for thermal-hydraulics ranging from the strand diameter ($<\sim 10^{-3}$ m), to the CICC length in a coil (up to several 10^2 m). On the other hand, taking advantage of this length-scale separation, the models presently used for CICC simulations are typically 1D (along the conductor) but they need constitutive relations (like friction and heat transfer coefficients) for the transverse mass, momentum and energy transport processes occurring between different conductor elements. The database for the transverse transport coefficients, unfortunately, does not appear complete, or free of internal contradictions, often because the smallness of the transverse scales makes even an experimental assessment of these processes difficult. Here we discuss these issues and possible strategies for overcoming some of the difficulties are proposed.

Keywords: Fusion magnets; Thermal-hydraulics; Superconducting cables

1. Introduction

ITER magnets use cable-in-conduit conductors (CICC), typically cooled by forced flow supercritical helium (SHe) at temperature $T_{op} \sim 5$ K and pressure $p \sim 0.6$ MPa.

Essentially all ITER coils, with the exception of a subset of the correction coils [1] use a dual-channel CICC, which has a central channel (hole, H) with preferential low impedance and a cable region (bundle, B) with large wetted perimeter, see Fig. 1.

Magnets are wound with one or more CICC. While the CICC are connected *electrically in series* through joints, which conventionally identify the longitudinal CICC boundaries, they are *hydraulically in parallel* to avoid heat accumulation affecting the high-field region.

Thermal-hydraulics plays a central role in superconducting coil technology. As a first example the appropriate use of heaters and thermal-hydraulic modeling as indirect diagnostic tools allowed the assessment of conductor degradation in the ITER Model Coils [2,3]. As a second example, the pressure-drop tests, in e.g. the ITER Central Solenoid Insert Coil (CSIC), gave first evidence of Lorentz-induced cable deformation (the so-called ''third channel'') in ITER CICC operation [4,5]. However, while the situation from the point of view of the ITER design criteria is possibly (albeit sometimes by chance) not unsatisfactory [6], we cannot be too happy with what we know

* Corresponding author. Tel.: +39 011 564 4490; fax: +39 011 564 4499.
E-mail address: roberto.zanino@polito.it (R. Zanino).

0011-2275/$ - see front matter © 2006 Elsevier Ltd. All rights reserved.
doi:10.1016/j.cryogenics.2006.01.007

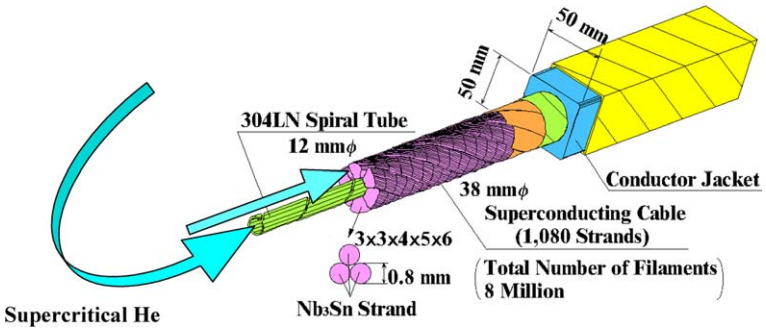

Fig. 1. Sketch of the CICC used for the ITER Central Solenoid Model Coil (CSMC) as representative of a typical ITER CICC. Note the dual-channel structure.

Table 1
Typical length scales in an ITER CICC

CICC component and dimension	Length scale (m)
Wrapping thickness (t_w)	10^{-4}
Strand diameter, spiral thickness (d_{St}, h)	$<\sim 10^{-3}$
Hole diameter, petal diameter (D_H, D_p)	10^{-2}
Sub-stage cabling pitch length (p)	10^{-1}
Coil curvature radius, short sample length (R, L_{SS})	10^{0}
Hydraulic length between joints (L)	10^{1}–10^{2}

today about ITER CICC thermal-hydraulics from a more fundamental point of view, which is our point of view in this paper.

The major length scales in a CICC are summarized in Table 1. One may note that $L_{\text{longitudinal}} \gg L_{\text{transverse}}$. This is used to justify the 1D (longitudinal) modeling approximation, which has been traditionally adopted since the early development of tools for the analysis of thermal-hydraulic transients in CICC (e.g., [7–9]), also because of its easier experimental validation. Constitutive relations for the *transverse transport fluxes* are then needed to close the set of fluid equations in the different cable elements.

Transverse inhomogeneities of the thermal-hydraulic parameters in the CICC lead to the transverse fluxes and they have been typically dealt with at the macro-element level, e.g., using multi-channel [10–12] and/or multi-conductor [13] models.

Transverse transport fluxes involve *friction factors* and *heat transfer coefficients*, for which correlations are needed (unfortunately, the short transverse length scales also imply much more difficulty in the experimental assessment of transverse processes).

Mass, momentum and energy transfer are typically (and also here) separated, but this separation is rather artificial, as the similar transport mechanism should be acting at the microscopic level, independently of the transported quantity. However, note that a particular but popular framework for the integrated treatment of friction and heat transfer (the so-called Colburn analogy, relating friction and heat transfer coefficients to their smooth-tube counterparts) was shown experimentally *not* to apply in the case of the central channel of a model ITER CICC [14].[1]

Finally, it may be worthwhile to note that a few approaches at truly multi-dimensional modeling of the ITER CICC have been presented in the past. Martinez [16] presented a global 2D home-made model for the whole CICC, with porous medium treatment of the bundle, but applied it only in the case of laminar flow. Feng [17] self-consistently derived a so-called quasi-2D CICC model, which is however still not validated, to the best of our knowledge. Inaguchi and co-workers [18] applied a global 2D model of the whole CICC based on commercial software (CD code) to the CSIC quench study; however, they try to explain friction in the central channel while neglecting the spiral thickness (which they are apparently forced to do because of CPU limitation arising from the attempt to treat the whole CICC), but the spiral is, on the contrary, the main cause for significantly increased friction with respect to the smooth tube, see [19] and below; this approximation makes therefore their model unfortunately irrelevant for ITER.

Here we stick to the traditional 1D approach, but an introduction to a first application of a *local* 2D/3D model, as a support to *global* 1D modeling, will also be presented.

2. Mass transfer

Mass transfer between cable bundle region and central channel allows the pressure relief in case of sudden heating of the strands and also contributes to access the central channel helium heat capacity by advective energy transfer [20]. The latter aspect is particularly important since separation/identification of the different mechanisms of energy transfer between the two regions is often unclear and source of some confusion as well.

[1] Also in the bundle region, the geometry and flow conditions do not guarantee a priori the applicability of the Colburn analogy, which was derived analytically for laminar flow on a plane surface and shown to be applicable also to turbulent flow on a plane surface or in smooth pipes but not applicable, e.g., to laminar flow in a pipe [15].

Direct experimental evidence on this phenomenon is unfortunately very limited because, generally speaking, the diagnostics, if any, of what happens in the central channel, are typically limited to one thermometer or so. To the best of our knowledge, only in the case of the QUELL conductor some more advanced measurement technique was applied, in order to diagnose density variations [21].

A rough (valve-like) model of radial transport in the CICC, relating the radial flow to the (square root) of the pressure gradient between bundle and hole regions is used in many codes (e.g., [10,11]), but it is not directly validated. The same is true for more complicated models [17].

3. Momentum transfer (friction factors *f*)

Momentum transfer between helium and solids determines, for a given mass flow rate, the pressure drop along the CICC and the related cost of pumping.

For the analysis, even in the simplest approximation adopted here, separate friction factors[2] are needed for the bundle region (f_B) and for the hole (f_H),[3] so that at least two sets of independent measurements are needed. Once f_B and f_H are known one can also compute the *flow repartition* in the CICC.[4]

Two different strategies have been developed for performing independent measurements. In both cases the pressure drop for given mass flow rate is measured in the CICC *with blocked central channel* (giving f_B), but the strategies differ as to f_H. In the first one, the pressure drop for given mass flow rate is measured in the standard CICC (giving f_H by subtraction), while in the second one, the pressure drop for given mass flow rate is measured in a spiral rib-roughened pipe (giving f_H).

It should be noted that both strategies rely on the assumption that the flow is the same with permeable or impermeable interface. Wraps, whenever present, and central spiral typically limit the possible interaction between the two flows, in particular from the point of view of momentum exchange (entrainment). In the second strategy outlined above, it is also assumed that the spiral geometry will be unchanged once it is in the real conductor. Also, as a possibly minor difference, the spiral gap is "attributed" to the bundle in the first case whereas it is attributed to the hole in the second.

Dimensional-to-dimensionless data conversion is obviously needed, going from pressure drop vs. mass flow rate to friction factor vs., e.g., Reynolds number. This conversion sometimes involves tricky choices, e.g., application or not of the traditional [22] 5/6 reduction in the strand wetted perimeter,[5] inner vs. outer diameter as hole hydraulic diameter, etc. While some of these choices may be arbitrary, other may give consistency problems, e.g., it is not obvious that *any* choice/definition of the central channel flow area A_H would allow reproducing the correct average flow speed V_H, starting from the measured volumetric flow rate $V_H A_H$ (both $V_H A_H$ and V_H could be *independently* measured in a heat slug propagation test in the central channel, but unfortunately such tests were never performed so far).

3.1. (Sub-)cable region *f*

The cable bundle region has been recognized as a porous medium-like structure long ago. Correlations for the friction factor f_B in the form used for pebble beds were derived [23], which are also adopted, in a slightly modified version [24], in the present ITER design criteria. These correlations are in the form

$$f_B = f_B(Re_B, \phi), \tag{1}$$

where Re_B is the Reynolds number, defined in terms of a hydraulic diameter $D_h^B = 4A_{fluid}^B/P_{wet}$, while ϕ is the void fraction (porosity), defined as A_{fluid}^B/A_{total}^B.

The correlation of Katheder [23]

$$f_B = (1/\phi)^{\alpha}(\beta/Re_B^{\gamma} + \delta), \tag{1a}$$

where $\alpha = 0.72$, $\beta = 19.5$, $\gamma = 0.88$, $\delta = 0.051$, was established for design/predictive purposes and the originally stated accuracy was between ±30% and ±70% against the database available at the time, which included only conductors without central channel and without wrappings. Consideration of the limited database available today from the tests of four different ITER samples with central channel blocked,[6] see Fig. 2, clearly shows that conductors with essentially the same void fraction, such as the PFCI ($\phi \sim 34\%$) and the CSMC ($\phi \sim 36\%$), show f_B different by about a factor of 2, at the same Re_B.[7] This consideration leads to an important question: are we missing a parameter

[2] In this paper we consistently use the so-called Moody (or Darcy) definition of the friction factor: $\Delta p/L = 1/2 f \rho U^2/D_h$.

[3] f_H and the respective Reynolds number Re_H are defined in this paper using the *inner* spiral diameter to compute both the hydraulic diameter and the flow area.

[4] This two-channel model is a simplification of the reality, as several different flow channels are actually present in an ITER CICC: as already mentioned above, a "third" channel naturally appears during coil operation because of Lorentz forces and finite cable stiffness, and also "triangles" appear on the CICC cross section at the contact between two petals and the (inner jacket) cable wrap, etc., but the analysis of these issues is beyond the scope of the present work.

[5] This was originally justified by assuming the core region of a triplet as inaccessible to the flow and as such not wetted, but it should also be observed that sometimes, in conductor cross sections, triplets are not that easily recognized/maintained as structures. It still is important, however, to guarantee consistency: if, for instance, a certain correlation was developed using the 5/6 factor in the dimensional-to-dimensionless conversion, that must be kept in mind once trying to compare one's own data with that correlation.

[6] CSMC short straight sample [25], Toroidal Field Model Coil (TFMC) short straight sample [24], Poloidal Field Conductor Insert (PFCI) short straight sample, with and without wraps [26].

[7] Note also from Fig. 2 that wrappings do not contribute significantly to the friction factor of the PFCI conductor [26], as opposed to what seen on EAST conductor tests [27], see also below.

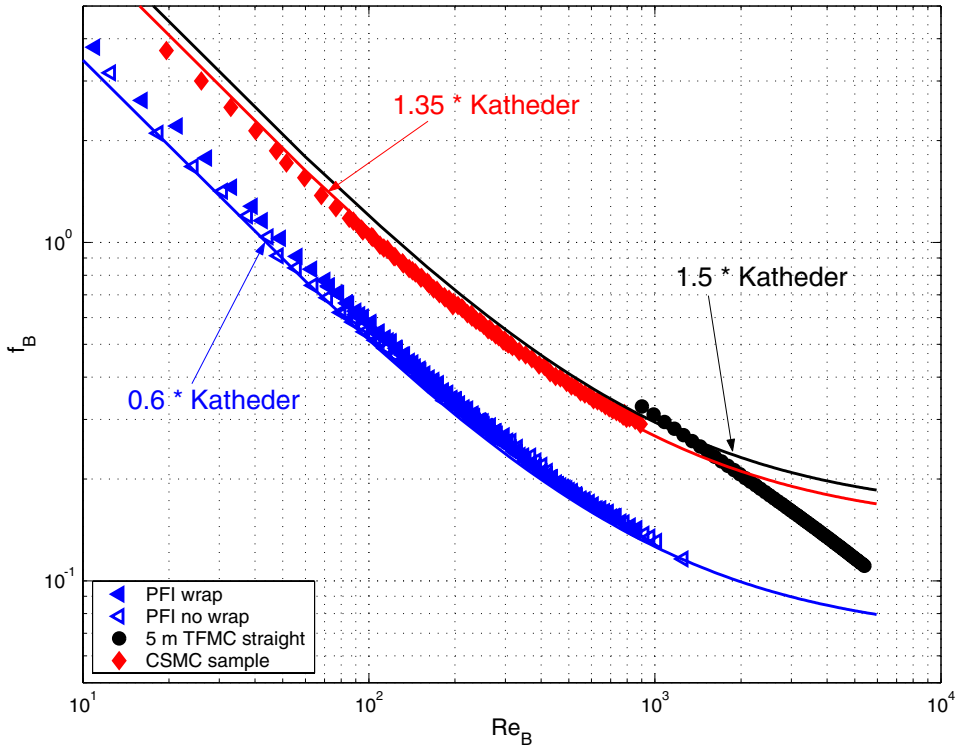

Fig. 2. Bundle friction factor as a function of the bundle Reynolds number for ITER conductors tested with blocked central channel: PFCI conductor with wraps (solid triangles), PFCI conductor without wraps (open triangles), TFMC conductor (circles) and CSMC conductor (diamonds). The data reduction accounts for the 5/6 coefficient, to be consistent with the friction factors resulting from the Katheder correlation, which are also reported, multiplied by a correction coefficient.

in the f_B correlation? Indeed, a correlation only depending on the porosity cannot be very accurate: according to such a correlation, a single-stage CICC, with the strands assembled all parallel in a spaghetti-like fashion, should have the same friction factor than a CICC with the same strands randomly twisted, but this cannot be true because the tortuosity of the coolant path will certainly affect the pressure drop.

In order to properly address the issue of friction *in the cable bundle region*, an extended database will be used here, including also conductor test results from non-ITER CICC characterized by the absence of the central channel, e.g., those used in the EAST [28] and KSTAR [29] tokamaks, as well as in the W7-X [30] stellarator. The inclusion of non-ITER conductors in this database is aimed at exploring a broader range of parameters (cabling patterns, etc.) than present in the ITER database strictly speaking, thus hopefully helping in identifying the most critical ones to be included in the correlation for f_B. Also (a subset of) the original Katheder database will be considered, which, for obvious historical reasons, does not include any ITER conductor strictly speaking.

The main features of the extended database are summarized in Table 2. It is seen that most of the tests were performed at room temperature (RT), using different fluids. Therefore, hydrodynamic similarity must be assumed to extrapolate to the relevant (cryogenic) ITER conditions. The whole database is shown in Fig. 3, wherein the conventional representation f_B vs. Re_B is used and Re_B is related to D_h^B. A rather significant dispersion of the data may be noted, even emphasizing the differences between the ITER conductors, which was shown in Fig. 2. The relative error for the different datasets is shown in Fig. 4 indicating that, while the predictive accuracy of the Katheder correlation is remarkably maintained also in the extended database (the original database including only the CICC from AIRCO 5 on in Fig. 4),[8] these errors are rather large (35–50% average-maximum error for the ITER CICC set alone). Therefore it is worthwhile attempting to correlate the pressure drop in the bundle using a more fundamental, porous-medium approach, which was pioneered by Long [14].

In a porous medium a generally accepted model for the pressure gradient is given by [31]

$$\overrightarrow{\nabla p} = -\frac{\mu}{K}\vec{\alpha} - \frac{J}{\sqrt{K}}\rho|\vec{\alpha}|\vec{\alpha}, \tag{2}$$

where μ is the fluid viscosity, K is the permeability of the porous medium,[9] α is the so-called seepage velocity

[8] The stronger disagreement in the case of W7X may be related to the peculiarities of the cabling pattern used for this CICC [30].

[9] At least in an ideal cable bundle, K should depend mainly on the so-called tortuosity of the medium, which in a CICC should reasonably depend in turn on the cabling pattern and on the pitches of the different cabling stages, as well as on spiral and cable diameters.

Table 2
Test conditions in ITER-relevant *bundle* friction database

Conductor (cabling pattern)	Nominal void fraction (%)	Fluid	p (bar)	T (K)	Re range	Comments	Source
CS1.2B ($3\times4\times4\times4\times6$)	36.3	H_2O	11	301	10–1000	Short straight sample	[P.Bruzzone]
TFMC ($3\times3\times5\times4\times6$)	36.9	N_2	30	273	600–7000	Short straight sample	[S. Nicollet]
PFCI ($3\times4\times4\times5\times6$)	33.5–34.3	H_2O	8	299–300	10–1000	Short straight sample wraps/nowraps	[C. Marinucci]
ABB-L	43	He	5	300	20–500		[H. Katheder]
Hitachi	39.9–46.6	–	–	–	400–42,000	$f(Re)$ only	
JA-DPC	37	–	–	–	300–22,000	$f(Re)$ only	
AIRCO 5,7 ($3\times3\times3\times7$)	47, 35	He	$\leqslant$17.2 (p_{in})	RT $\rightarrow$ 77	100–4000	$f(Re)$ only, 6 m sample	
US-DPC	43	–	–	–	80–800	Correlation only	
WSTGH	40.5	–	–	–	40–10,000	Correlation only	
KSTAR TF00 ($3\times3\times3\times3\times6$)	32	He	5.3 (p_{in})	5	~4000	No central channel, Limited subset	[K. Kim]
KSTAR CSMC ($3\times4\times5\times6$)	37		4.5 (p_{in})	5	~4000		
EAST ((2+2)$\times3\times4\times5$+1)	36.7–38.4 37.3	N_2 He	1.1 (p_{out}) 5 (p_{in})	RT 5.1–5.4	300–3000	$N_2\rightarrow$ 4 short samples, 2 wraps/2 nowraps, He $\rightarrow$ TF5, nowraps, No central channel, Limited subset	[H. Bai, P. Weng]
W7X ($3\times3\times3\times3\times3$)	37 ± 2	He	1 (p_{out})	RT	10–150	Double layer on spool, No central channel, Limited subset	[K. Risse]

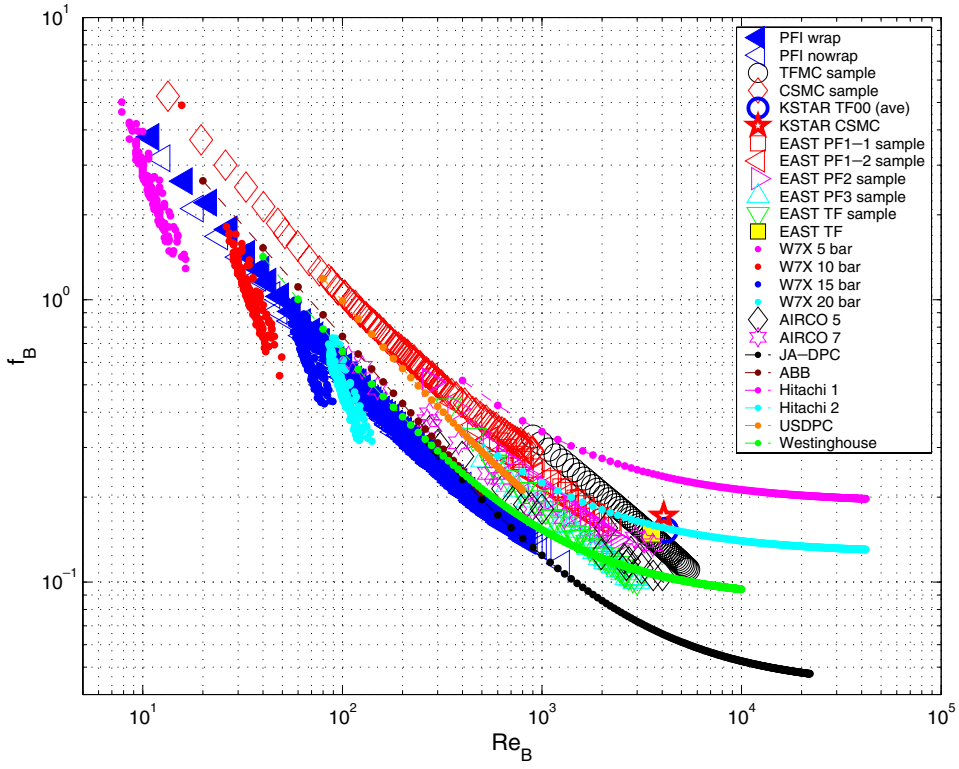

Fig. 3. Bundle friction factor as a function of the bundle Reynolds number derived from the experiments on the samples listed in Table 2.

(i.e., the velocity averaged over a representative elementary volume, *including both the fluid and the solid phase*), J is the inertial constant and ρ is the fluid density. The linear term in (2) is the well-known Darcy contribution (friction drag), whereas the quadratic term is the so-called Forchheimer contribution (form drag). We may rewrite (2) in the 1D case we are interested in (coordinate x along the CICC), introducing the fluid flow velocity u (averaged over a volume *including only the fluid phase*) in x direction, which is related to the seepage velocity by the Dupuit–Forchheimer relation $\alpha_x = \phi u$. We have then

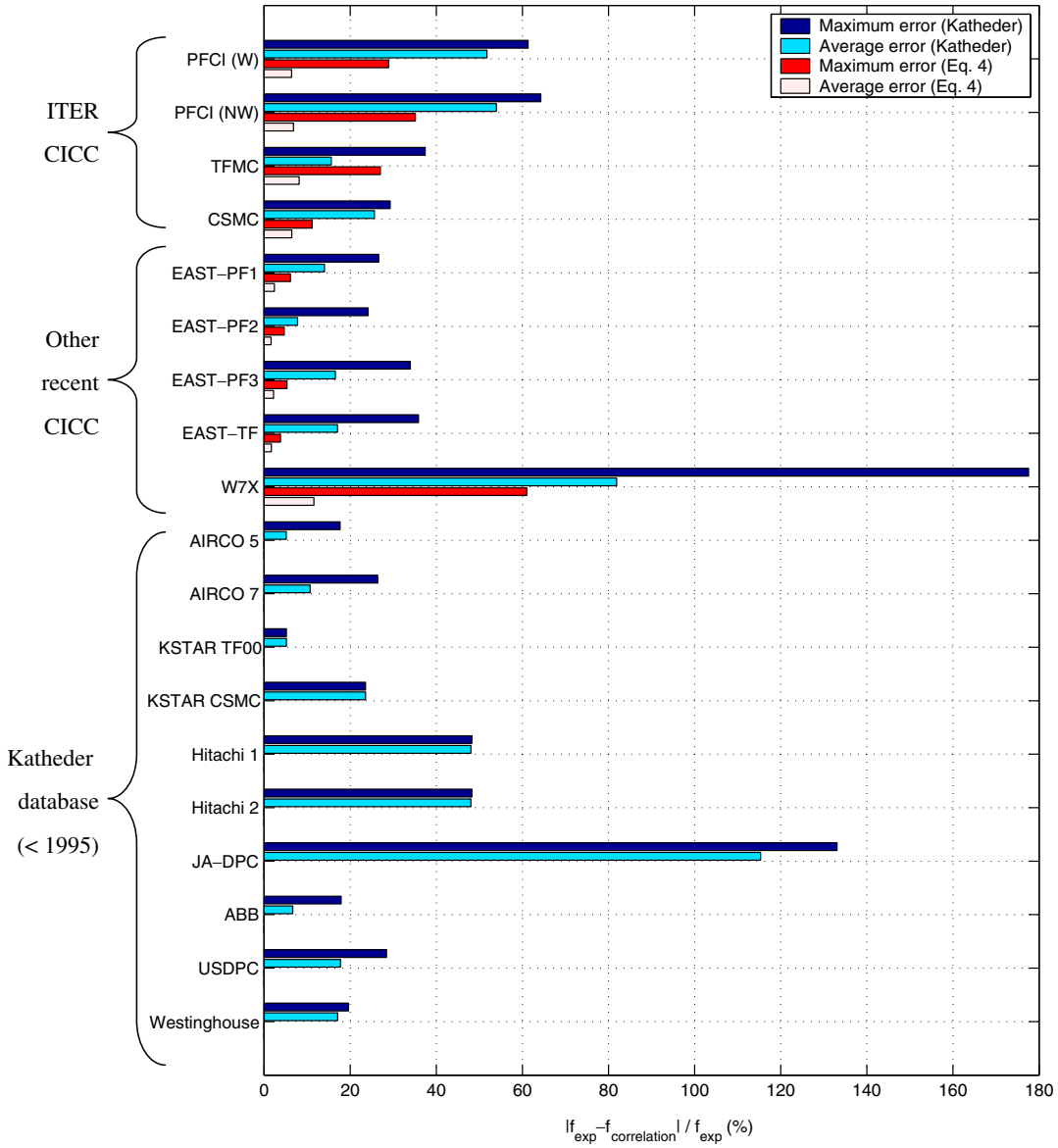

Fig. 4. Maximum and average relative error (normalized with respect to the experimental data) of the different data set with respect to the Katheder correlation and, where applicable, with respect to correlation in Eq. (4).

$$\frac{\partial p}{\partial x} = -\frac{\mu}{K}\phi u - \frac{J}{\sqrt{K}}\rho\phi^2 u^2. \tag{3}$$

This relation can be integrated along the CICC length L under two different simplifying assumptions: either incompressible flow is assumed, which will be applicable to, e.g., the H_2O test results, or Fanno flow (compressible, 1D, isothermal flow of a perfect gas) is assumed, which will be applicable to, e.g., the He and N_2 RT test results. The result of the integration can be summarized in dimensionless terms by the deceptively simple relation:

$$f_K = \frac{1}{Re_K} + J, \tag{4}$$

where the friction factor and Reynolds number are defined (using the square root of permeability as length scale instead of the hydraulic diameter), respectively, as

$$f_K \equiv \beta \frac{\Delta p}{L} \frac{\sqrt{K}\rho_{out} A_{fluid}^2}{(dm/dt)^2} \frac{1}{\phi^2}, \tag{5a}$$

$$Re_K \equiv \frac{(dm/dt)\phi\sqrt{K}}{\mu A_{fluid}}, \tag{5b}$$

$\beta = 1$ for incompressible flow (whereas $\beta = \langle p\rangle/p_{out} = (p_{in} + p_{out})/2p_{out}$ for Fanno flow), ρ_{out} is the fluid density at the outlet of the test section, dm/dt is the mass flow rate.

It is seen that (4) predicts, for any (!) CICC bundle (independently of the details of its internal structure), a linear dependence of the *suitably defined* f_K on $1/Re_K$. It is known [31] that the permeability K depends on the medium porosity and geometry but, unfortunately, there is no obvious way to compute the permeability K from the medium geometry except in very simple cases, which are hardly relevant for the case at hand. Concerning the inertial constant

J, it is known that this is actually not a constant but may depend also on the medium geometry, as well as on pore-scale turbulence [31], but this term is otherwise even less known than K. Indeed, the only potentially practical way to compute K (and J) in an ideal bundle geometry is through CFD calculation, correlating a posteriori the mass flow rate computed for a given pressure gradient with the pressure gradient itself, see below.

In view of the above, we use the pressure drop data to find, for the subset of CICC in the database for which all needed input is available to us, the values of K and J best fitting the measurements. These values are collected in Table 3 while the result of correlation (4) is shown in Fig. 5.

It is seen in Table 3 that the deduced K's vary by a factor of ~4 notwithstanding a range of porosities different by at most ~15%! An even larger variation of J, by about a factor of 10, may be noted. These variations obviously reflect the above-mentioned significant differences in the hydraulic characteristic of the different CICC. Both K and J turn out to be in the same order of magnitude assessed in the past on somewhat different cables [14].

Table 3
Best fitting K and J from pressure drop tests

Conductor	Void fraction ϕ	K (m^2)	J
PFCI (w)	0.335	2.80E−09	7.57E−02
PFCI (nw)	0.343	3.80E−09	7.34E−02
CSMC	0.363	3.10E−09	1.14E−01
TFMC	0.369	1.10E−09	1.56E−02
EAST PF1 (w)	0.367	1.60E−09	3.34E−02
EAST PF2 (w)	0.367	1.60E−09	2.84E−02
EAST PF3 (nw)	0.384	2.80E−09	1.99E−02
EAST TF (nw)	0.373	2.30E−09	1.87E−02
W7X	0.370	3.70E−09	1.25E−01

Quite obviously, the direct comparison (in terms of accuracy) between (4) and Katheder's correlation, see Fig. 4, is partly unfair, because the former is mainly interpretive in nature, while the latter confirms its predictive purpose, although error bars are rather large. Predictive use of (4) would require an a priori determination of K and J, which is presently beyond our capabilities.

3.2. Central channel f

Early attempts to correlate the pressure drop with the mass flow rate in the QUELL CICC central channel assumed $f_H = \alpha_{f_H} \times f_{smooth}(Re_H)$ [32]. However, tests of different TFMC pancakes at Ansaldo showed that details in spiral design (in particular the gap size g) could significantly affect the pressure drop [33]. This was eventually confirmed both in the CSMC operation (MIT circular wire vs. flat spiral) [34] and in the TFMC operation [35]. In this sense, a fundamental understanding of the friction in the central channel could in principle allow the optimization of the spiral (for instance, minimizing the pressure drop while keeping sufficient heat exchange and pressure relief capabilities), subject to mass, momentum, energy transfer and mechanical constraints, as well as to the presence of the wraps.

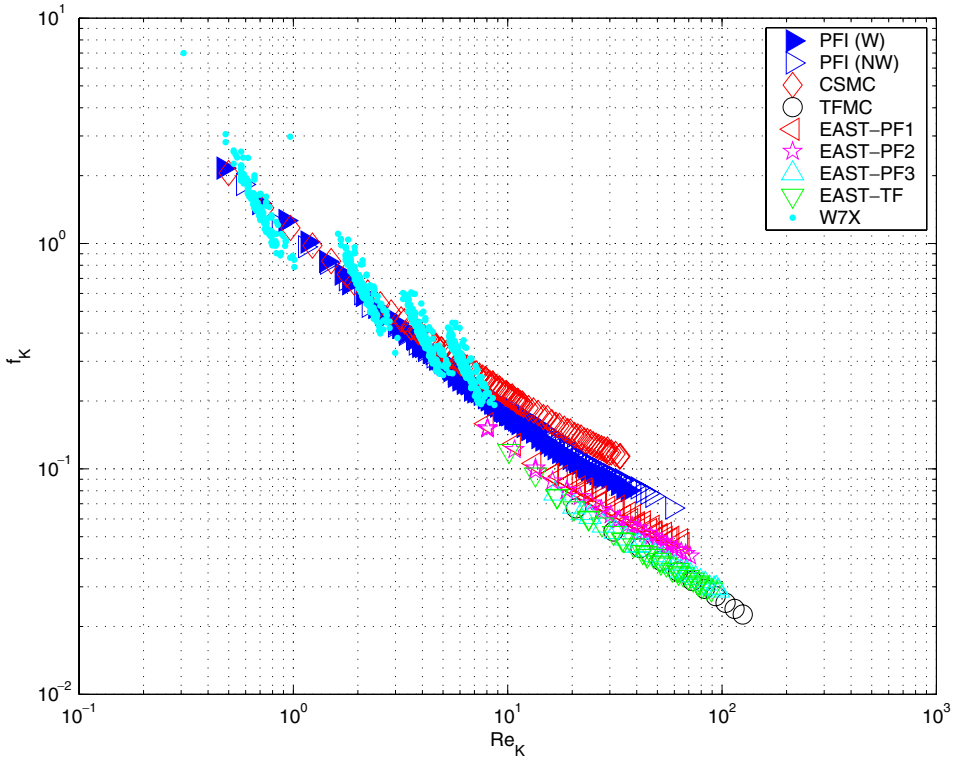

Fig. 5. Friction factor, as defined in (5a), as a function (4) of the Reynolds number, as defined in (5b), deduced from test results of a sub-set of the samples listed in Table 2.

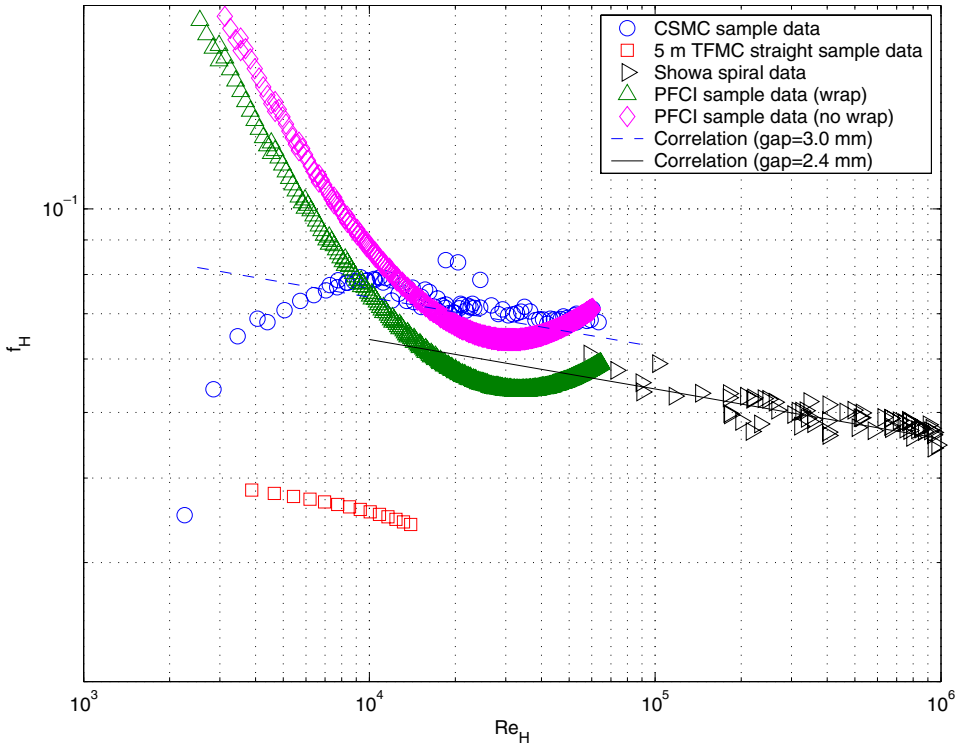

Fig. 6. Hole friction factor as a function of the hole Reynolds number measured on different ITER conductor short samples (symbols) and compared with available correlation [19] (lines)

CEA started testing of spiral rib-roughened pipes in the OTHELLO facility using pressurized N_2 at RT during 1999, providing least square fits *for each spiral* in the database [33].

From the same database (3 spirals with different gap *but same diameter* $D_{in} \sim 10$ mm) a general correlation *for all spirals* in the database was developed, including g/h as additional dimensionless parameter [19] in the form

$$f_H = f_H(Re_H, (h/D \text{ fixed}), \mathbf{g}/\mathbf{h}), \tag{6}$$

and validated [36] on CSMC straight sample data.

Unfortunately, the limited database available at present on f_H is not free of contradictions. For instance, derived data for f_H from the TFMC straight sample differ by a factor of ~2 from TFMC spiral data, see Fig. 6. In Fig. 6 we may also note that the results of the PFCI sample are in the same ball park as the CSMC sample and the TFMC spiral data over a certain range of Re_H, notwithstanding a smaller value of the gap (~1.7 mm for the PFCI [39] vs. 2.4–3.0 for CSMC-TFMC[10]). Also, at decreasing Reynolds f_H tends to increase in the PFCI case whereas it decreases in the case of the CSMC sample, suggesting that either data are not reliable for $Re_H < 10^4$. Finally, the spread between PFCI data with and without wraps may only be attributed to measurement inaccuracy, as the central channel is the same in these two cases (more mixing between the two channels in the case without wraps should not happen anyway, because at steady state the local radial pressure gradient driving the flow between the two should vanish, both with and without wraps).

In view of the proposed use in ITER of CICC with a smaller central channel ($D_{in} \sim 7$ mm for the CS and TF coils [1]) CEA recently started performing tests of new spirals based on which we aimed at assessing if there is any explicit dependence of the friction factor on the relative roughness h/D

$$f_H = f_H(Re_H, \mathbf{h}/\mathbf{D}, g/h). \tag{7}$$

These tests were performed both in the OTHELLO facility (which uses pressurized N_2) and in the HECOL facility (using pressurized H_2O). Unfortunately, several problems have been encountered during the evaluation of the data concerning, e.g., smooth-tube validation, hydrodynamic similarity, dependence on flow direction. It may therefore be concluded that, concerning friction in the central channel, the experimental database available today appears insufficient to draw any conclusions in the form of generally applicable correlations of the type given in (7), so that such a *predictive* correlation for f_H is not available at present [40].

[10] Some uncertainty exists as to the actual gap width in one very popular spiral (the so-called Showa) used for some of the TFMC pancakes as well as for some of the CSMC layers. While the original measurement for the spiral alone gave 2.4 mm [33], on which all correlations for f_H are based, measurements performed during the conductor QA resulted in ~3.0 mm [37] and very recent examination of ~10 pitch lengths in the CS1.2B conductor gave a range 2.7–3.0 mm [38]. Therefore, at least a ±10% uncertainty around an average of 2.7 mm should be considered, based on the whole set of dimensional checks above.

We shall see below that advanced computational fluid dynamics (CFD) methods are being proposed to address the problem of friction in the central channel (as well as others in ITER CICC thermal-hydraulics, see above) and can be applied, of course within their own limitations, to help overcome at least some of the above difficulties.

3.3. Global *f*

The above results should be used in the end for at least two "practical" purposes, which are obviously not independent: (a) to determine the pressure drop on the conductor for a given total (bundle + hole) mass flow rate, (b) to assess the flow repartition between the two channels. Details of this approach and implications for the ITER design criteria are discussed in [6].

If we rely on the correlation of Katheder for f_B and we assume we have a perfect correlation for f_H, the error bars in f_B, see Fig. 2, result in an uncertainty of pressure drop and flow repartition as shown in Fig. 7. It may be noted that for the range of multipliers relevant for ITER conductors (see Fig. 2) a decrease of f_B obviously leads to a increase of the flow fraction in the bundle as well as, because of the simultaneous reduction of the flow fraction in the hole at constant total mass flow rate and f_H, to a decrease of the pressure gradient. It should also be noted that the range of uncertainties (Katheder multipliers) shown for ITER conductors in Fig. 2 corresponds to a rather significant uncertainty of up to 40–50% in the pressure drop and up to ±5% (absolute) in the flow fraction in the bundle.

It was already noted in the past that the comparison of different data (including 3-turn samples) of the TFMC conductor seems to indicate an effect of conductor curvature, leading to an ~50% larger f for both the TFMC and the 3-turn samples, if compared with the straight sample [36]. In view of their singularity, we also checked the TFMC straight sample data (where N_2 was used), but they appear to be confirmed by data collected, again at CEA, on another straight TFMC sample using H_2O, see Fig. 8. Note that correlations for curved pipes, e.g., Ito's [41], predict an increase of the pressure drop scaling with the parameter $[Re(r_{cond}/r_{curv})^2]$, where r_{cond} is the channel radius and r_{curv} is the curvature radius of the coil (i.e., irrelevant for the bundle flow if compared with the central channel, in view of the much smaller hydraulic diameter); these correlations, however, give at most a 10% correction or so, i.e., not enough to explain the above-mentioned differences in the case of the TFMC.

However, the curvature effect seems not confirmed by CSMC data (although from the point of view of curvature it should be at least as affected as the TFMC, which has locally smaller curvature radii but also long straight legs), see Fig. 9, where CSMC 1A data (obtained using He in cryogenic conditions) [34] appear to fall on a reasonable extrapolation of CSMC straight sample data (obtained using H_2O at RT) [25].

The forthcoming test of the PFCI should hopefully help in clarifying the curvature issue by comparing results of pressure drop tests with those obtained on a PFCI short sample (without blocking the central channel) [39]. Also tests from other conductors (e.g., W7X) or perhaps

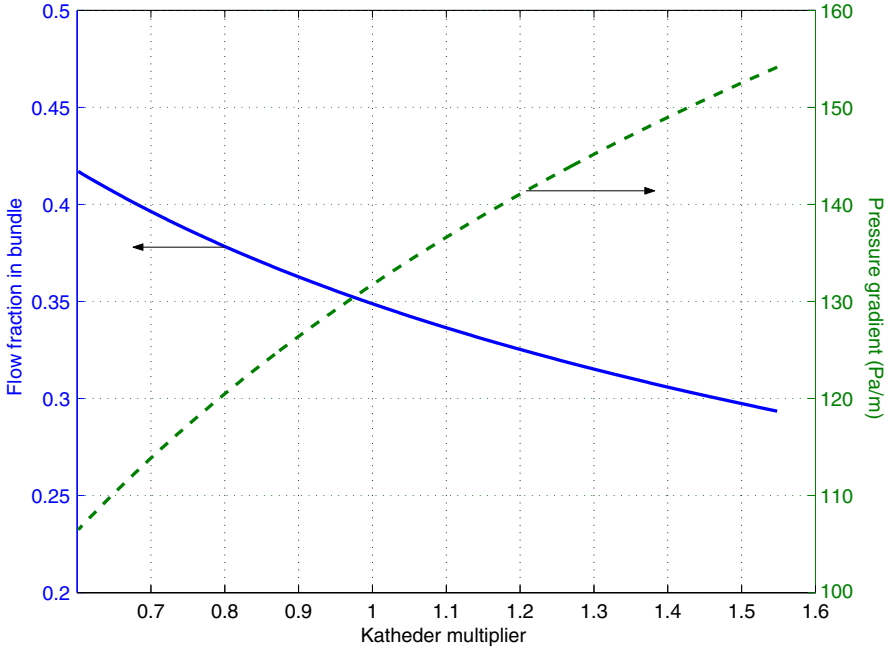

Fig. 7. Sensitivity of the pressure gradient and of the flow repartition between bundle and hole on the uncertainty on f_B (quantified by the chosen multiplier of the Katheder correlation) at given total mass flow rate (10 g/s He @ 5 K, 5 MPa). TFMC conductor data and f_H correlation as in [19] were assumed.

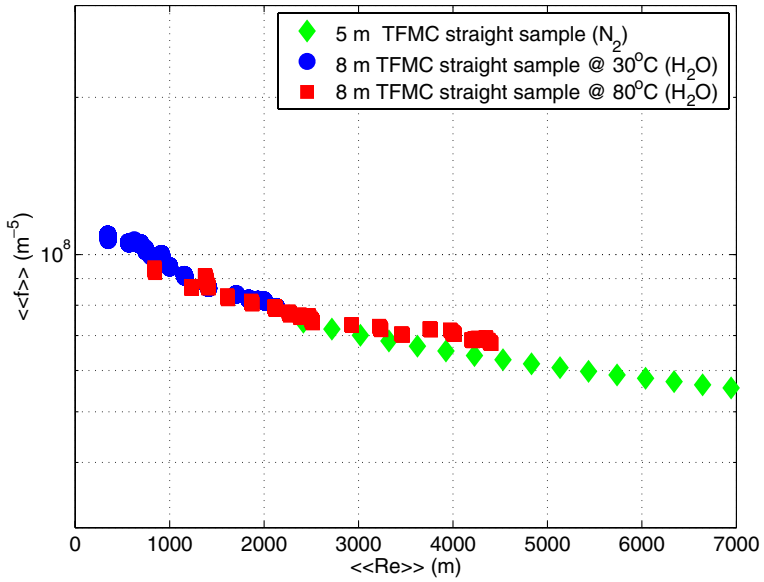

Fig. 8. Total friction "factor", as defined in [36] as a function of the total Reynolds "number", as defined in [36], for the TFMC straight sample tested with N_2 (diamonds), with water at 30 °C (circles) and with water at 80 °C (squares).

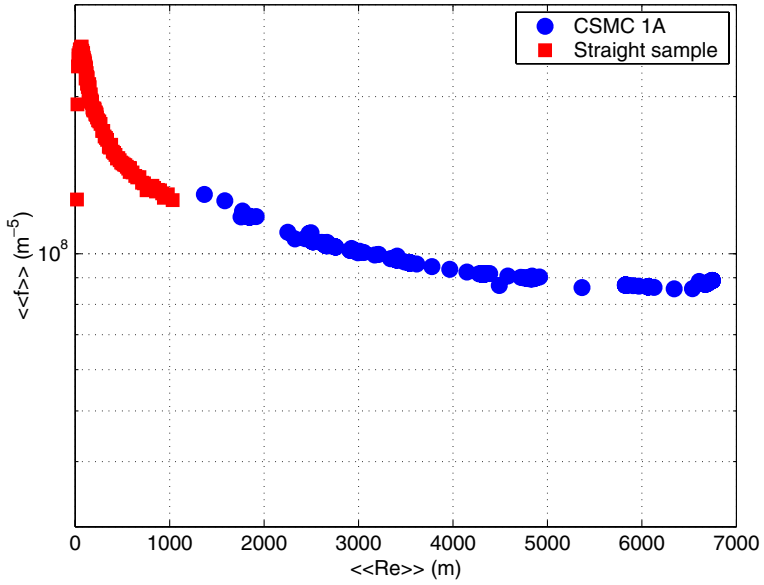

Fig. 9. Total friction "factor", as defined in [36] as a function of the total Reynolds "number", as defined in [36], for the CSMC conductor; results from conductor 1A test (circles) and from the straight sample test (squares).

dedicated tests of *curved* conductors *with blocked central channel* could be used to track which, if any, of f_B and/or f_H may be affected by curvature.

4. Energy transfer (heat transfer coefficients *h*)

The major heat transfer processes in a CICC are summarized in Fig. 10, emphasizing the different conductor components involved: bundle region helium, hole region helium, strands, jacket. Heat transfer significantly affects, together with friction, the most relevant time scales of thermal-hydraulic transients in CICC [42]. The single heat transfer processes are considered below.

4.1. Strand–helium h (transient and steady state)

The heat transfer coefficient between strands and helium (h_{St-He}) enters the stability (Stekly) condition [43].

h_{St-He} is modeled in the codes as series of $\min(1/h_t, 1/h_{Nu})$ and Kapitza resistance, where h_t and h_{Nu} identify the transient and steady state components, respectively, of the heat transfer coefficient.

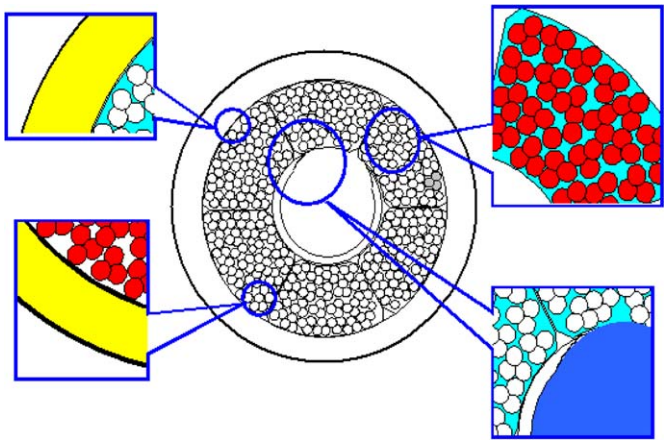

Fig. 10. Different heat transfer channels in an ITER CICC: strand–He (upper right), bundle He–hole He (lower right), strand–jacket (lower left), bundle He–jacket (upper left). A four-temperature model (jacket uniform, all strands common and uniform, bundle He uniform, hole He uniform) is implicitly assumed in this representation.

Transient heat transfer (h_t) can be modeled at different levels of sophistication [44]. In the simplest approach we may consider the thermal boundary layer of thickness $\delta_f(t)$ forming at the strand surface because of sudden (step) heating of the strand and then propagating inside the fluid at a rate related to the fluid thermal diffusivity α_f, until thermal and flow layers become comparable (steady state heat transfer condition). As a thermal boundary layer has not been established yet during the transient phase, the heat transfer coefficient may be deduced assuming pure conduction with conductivity k_f through the forming boundary layer, while $\delta_f(t)$ can be assessed as the length scale in the fundamental solution of the transient heat conduction problem. Therefore, we have

$$h_t \sim \frac{1}{\frac{\delta_f}{k_f}} \sim \frac{1}{\frac{\sqrt{\alpha_f t}}{k_f}} = \sqrt{\frac{k_f \rho_f c_{p,f}}{t}}. \quad (8)$$

Steady-state heat transfer (h_{Nu}) is derived from correlations for the Nusselt number Nu (Re, Pr) and the Dittus–Boelter correlation is typically used, giving $h_{Nu} = h_{DB} \sim$ several 10^2 W/m^2 K. However, it should be noted that, strictly speaking, application to our case (essentially heat transfer between solid and fluid phase of a porous medium) of the Dittus–Boelter correlation, which was derived for pipes, is somewhat unjustified. Furthermore, it was already noted in the past, see, e.g., [45,46], that $h_{Nu} \sim$ several 10^3 W/m^2 K appears needed in several applications. Even in this case, as for the friction coefficient in the bundle region discussed above, correlations for porous media not in thermal equilibrium between the phases, see, e.g., [47], may indeed result in more appropriate values, up to 1 order of magnitude larger than h_{DB}.

Kapitza heat transfer, which is related to the "interfacial thermal boundary between any two dissimilar materials where electronic transport does not contribute" [48], is modeled as $h_K = 200(T_{St} + T_{He})(T_{St}^2 + T_{He}^2)$. Simple verification shows that the Kapitza thermal resistance is typically negligible at ITER operating conditions ($T > \sim 5$ K) since $h_K > \sim 10^5$ W/m^2 K.

4.2. Strand–jacket h

Provided there is sufficient contact between strands and jacket (which is typically the case except on the high-field side of a conductor because of Lorentz forces inducing sometimes significant deformation of the cable and its detachment from the jacket), the heat transfer coefficient between strands and jacket (h_{St-Jk}) contributes:

- The second, after h_{St-He}, parallel channel for direct strand cooling (but the strand contact perimeter $\sim f_{contact} P_{Jk}$ is $\sim$ two orders of magnitude lower than the strand wetted perimeter).
- A channel for accessing the jacket heat capacity in the later quench phase. *Above 30 K*, indeed, the jacket heat capacity in the CICC is about an order of magnitude larger than the helium heat capacity. Therefore, the time scale $\sim 1000/(h_{St-Jk} f_{contact})$ *s* could be relevant (see below) for quench propagation and hot spot temperature.
- The only direct channel for strand *heating*, if the jacket is heated first by, e.g., a heater as, for instance, in the case of the Insert Coil stability tests [46] (here a possible selective heating in case of cable deformation should also be taken into account).

Direct experimental knowledge of h_{St-Jk} is unfortunately very limited. Values up to 2500 W/m^2 K were recently measured [49] but @ relatively low mechanical load (<30–40 kN/m) with respect to the operating ($I \times B$) peak load of ITER conductors. Values assumed so far in the simulations are therefore most likely arbitrary.

Finally, let us note that, at least to the extent that they are both related to contact resistance issues, h_{St-Jk} is also relevant for the heat transfer coefficient between strand and strand h_{St-St} needed in the case of multi-solid models, which are not discussed here in detail.

4.3. Jacket–helium h

The heat transfer coefficient between helium and jacket (h_{Jk-He}) is relevant for several issues and namely:

- Analysis of stability tests and resistive heater tests.
- Interpretation of the jacket temperature sensor signals.
- Access to the jacket heat capacity in the later quench phase (but the corresponding time scale may be longer than that estimated above for h_{St-Jk} because of stagnating He in the hot spot region).

From the porous medium point of view, h_{Jk-He} should be in principle different from h_{St-He} because the different (lower) porosity close to the jacket [31] leads to a different flow pattern and therefore to different heat transfer [47].

4.4. Helium–helium h

The most important heat transfer mechanism between helium and helium affects the heat transfer coefficient between bundle and hole region h_{BH}, which contributes to determine the time scale on which the central channel helium heat capacity becomes accessible for cooling the strands. This is not relevant (it is too slow) for stability, but it is important for, e.g., re-cooling of the coil after transient events (AC losses), and/or quench propagation.

A longtime interest for this topic exists, related to heat slug propagation in a dual-channel CICC [50,51]. Very recently, the problem has been reconsidered, following different approaches and making use of new experimental data available from the test of short samples. We refer to that literature for details [52–54].

The helium–helium heat transfer problem appears more critical, in perspective, for multi-channel modeling, where, e.g., the issue of heat transfer *between sub-channels*, for instance between petals, see below, must be considered, or even worse, between artificial channels (without real physical boundaries like the sub-cable wraps). The latter situation is relevant to the case when the description/discretization of the CICC cross section should go below the last but one stage and possibly down to the single strand level [12].

5. Comments on the present design criteria

We present here just a brief summary of the above-mentioned issues, as seen from the point of view of the ITER design criteria.

Transverse (*bundle/hole*) *mass flux* is presently not included in the design criteria.

For the case of the *pressure drop* (*friction*) a detailed discussion is already given in [6].

Instead of attempting a first principle approach, in the design criteria the Stekly criterion is assumed valid and values of h_{St-He} have been deduced from experimental data *of stability margin*. One disappointing implication of this approach is that different h_{St-He} are presently foreseen for different SC material, which is obviously unjustified from a purely thermal-hydraulic point of view.

None of the other above-mentioned heat transfer coefficients – between strands and jacket (h_{St-Jk}), between helium and jacket (h_{Jk-He}), or between bundle and hole region (h_{BH}) – enters the present design criteria.

6. Special problem areas

Under this heading we collect a couple of selected thermal-hydraulic problems, which in a sense combine the previous items into a (more) complex picture.

6.1. Buoyancy effects

In the case of a vertical tract of a CICC (like it may occur in the TF coils, but also presently in the Sultan short samples), localized heating of a portion of the CICC (typically the He in the bundle region cooling the strands heated by neutrons and/or by AC losses) may result, in the case of originally down-flowing coolant, in stagnation/backflow of the coolant in the annular region combined with increased down-flow in the central channel. In this situation, although the total (forced) mass flow rate would be maintained, heat transfer in the cable region could be compromised, seriously affecting the CICC performance. Indirect evidence of these phenomena was indeed provided by temperature measurements in Sultan short samples at sufficiently high input power [55]. Simulation results, however, were only in qualitative agreement with the measurements, in view of the very complex interplay of local heat and mass transfer phenomena both along and across the CICC, over very short length scales (10^{-2}–10^{-1} m, in the case of AC-loss-induced buoyancy in a Sultan sample) [56]. More recently, the similar phenomena were investigated in another Sultan sample [57].

The potential relevance of buoyancy for ITER TF operation (where it might be induced by nuclear heating of the inner leg) turned out to be doubtful according to simple modeling [58] but is now under more detailed evaluation [57,59].

6.2. Transverse temperature gradients

Most of present-day codes are one-dimensional, as seen above, so that temperature gradients are assumed to exist only in the axial direction (along the CICC). Because of their different proximity to the strands, a possible temperature difference between helium in the cable region and helium in the central channel (both assumed separately uniform) was hypothesized, but temperature measurement in the central channel is not easy/customary except in dedicated experiments, so that experimental evidence in this field is somewhat scattered.

Indeed, a ΔT *between central channel and jacket* was measured, e.g., in the USP joint and also simulated [60], while a ΔT *between central channel and annulus* was measured in HECOL tests at CEA [61]. ΔT *between petals* was measured in the GJ conductor [62] and simulated semi-quantitatively [63] with the M&M code.

Clearly, transverse ΔT between different cable components, even at the sub-petal level, may be particularly relevant in the case of coupled electro-magnetic thermal-hydraulic transients (e.g., a local normal transition in NbTi CICC in the form of "sudden quench"), as discussed above for the single heat transfer coefficients [67].

7. CFD modeling of thermal-hydraulic phenomena in ITER CICC

It was seen above that several uncertainties affect transverse transport (be it mass, momentum or energy) in CICC while, on the other hand, 1D models are already sufficiently computationally intensive to make a multi-dimensional

treatment of the whole CICC unpractical. Therefore, we propose here a novel approach:

- Assess the *radial*/transverse transport with *local* 2D/3D (Reynolds-Averaged) Navier–Stokes models.
- Determine by post-processing the resulting constitutive relations.
- Apply these relations in 1D *axial* but *global* models.

Here only an introduction to a first step in this direction is given, devoted to the issue of friction in the central channel (details and validation of this step are reported in [64]). This approach, in view of its potentially modular nature, shall then be extended elsewhere to transverse heat and mass transfer, friction in the annular region, etc.

We use the FLUENT commercial code for detailed 2D/3D flow modeling in the central channel: for any given pressure drop Δp the mass flow rate is *computed* by the code integrating the axial flow field across the CICC and compared with experimental results. This corresponds in a sense to performing a computational experiment. From the results of several runs (i.e., several different Δp) a computational hydraulic characteristic of the central channel can be determined from which the friction factor vs. *Re* and geometry can be *computed*. In other words, f is in such 2D/3D computation an output parameter as opposed to the 1D computation where it is needed in input.

Just to give an idea of the approach, we consider a 2D model of the spiral (simulated in this case by repeated/periodic annular ribs), see Fig. 11 which shows the computed streamlines inside the gap for two different turbulence models. The results confirm the *critical sensitivity of the prediction to the turbulence model chosen*, which is well known in the literature on separation and reattachment problems, see, e.g., [66]. As discussed in [19], the shorter the predicted reattachment length is, the higher the friction.

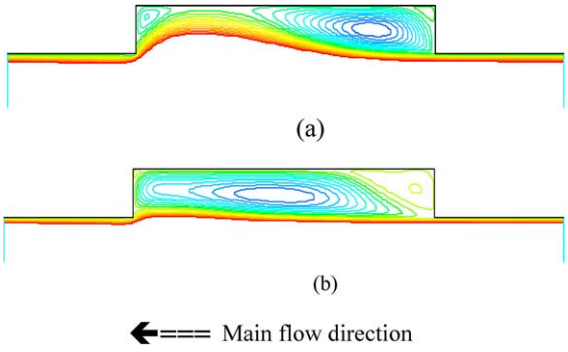

Fig. 11. Numerical solution (streamlines) of the 2D model @ $Re \sim 10^5$ obtained using the k–ε turbulence model [65] (a), with resulting dm/dt 0.34 kg/s, or the k–ω turbulence model [66] (b), with resulting dm/dt 0.51 kg/s, for the same given pressure drop and mesh. The computational domain includes half annular rib width on each side of the gap where a major re-circulating vortex is formed (a zoom of the region close to the wall is shown, excluding most of the central channel). Periodic and axially symmetric conditions are assumed for the incompressible flow of H_2O at RT conditions. Main (imposed flow) is from right to left.

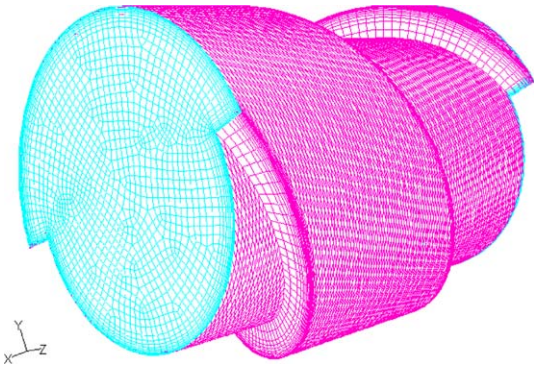

Fig. 12. Example of a 3D computational grid (only surface elements are shown) for the study of spiral friction. Domain length is one spiral pitch.

It may also be worthwhile to note that, in this 2D simulation at least, the so-called form friction (proportional to the fluid pressure at the wall) dominates on the viscous friction (proportional to the velocity shear at the wall).

This simple 2D analysis can obviously be extended by considering the more realistic, full 3D problem, for which the (ideal) geometry and meshes similar to that shown in Fig. 12 can be used. With respect to the previous 2D case, this analysis aims at the assessment of swirl flow possibly induced by the spiral, as well as of possible preferential channeling along the spiral gap. Again, a periodic structure is assumed in the simulation, so that the considered computational domain can be reduced to a spiral pitch length.

8. Conclusions and perspective

Although ITER CICC's work, thermal-hydraulics in ITER CICC is perhaps less understood, from a fundamental point of view, than it could be expected after many years of research.

Thermal-hydraulic issues in ITER CICC are summarized by friction factors and heat transfer coefficients, which enter the lumped-parameter description of transverse fluxes used in the present codes. These codes are routinely used to analyze thermal-hydraulic transients that are intrinsic to the operation of such systems, but of course, they depend heavily on the availability of accurate coefficients for the set of equations they solve, as the simulation results will never be more accurate than the input.

The main issues identified in this paper can be roughly summarized as follows:

- *Transverse (bundle/hole) mass flux*: not well known. Further work (both experimental and theoretical/modeling) is needed to understand this possibly important coupling mechanism between the two main regions of an ITER CICC.
- *Friction factor in the cable region* f_B: available predictive correlations, depending on void-fraction only, lead to errors $> 60\%$ in some cases. Based on the porous medium approach we have proposed an improved

correlation, Eqs. (4) and (5), in terms of permeability and inertial constant. The latter have however to be determined either experimentally case by case or they could be assessed computationally in idealized geometry for predictive purposes. An improved predictive correlation is therefore still missing.

- *Friction factor in the central channel* f_H: available correlations fit well only a sub-set of the data. The database is partially internally inconsistent. Extended data (at different spiral diameters) and modeling effort are needed to take advantage of the potential for optimization of spiral design, as well as for understanding the physics of friction in this region.
- *Heat transfer coefficients*: experimental work directly addressing the measurement of h_{St-He} in ITER CICC is presently missing, so that correlations typically used for this basic heat transfer mechanism come from available literature in other fields of application; for h_{Jk-He} the situation is similar, while limited available work on h_{St-Jk} should be extended to peak load conditions in ITER; much new work has become recently available on h_{BH}, although a correlation is still missing.

The use of local multi-dimensional CFD modeling of thermal-hydraulic transport processes in a CICC is advocated as an alternative means to obtain constitutive relations and assess the respective transport coefficients. Hints at a first application of this novel approach to the problem of friction in the central channel were given.

Acknowledgements

The European Fusion Development Agreement (EFDA) and the Italian Ministry for Education, University and Research (MIUR) partially financially supported this work.

We are also grateful to H. Bai (IPP-CAS), P. Bruzzone (CRPP), H. Katheder, K. Kim (KBSI), C. Marinucci (CRPP), M. Nagel (IPP Garching), K. Risse (IPP Garching), P. Weng (IPP-CAS) for discussions and for making their data available to us. Finally, we wish to thank one of the anonymous referees for a very careful and critical reading of the manuscript, providing many helpful suggestions aimed at improving the readability of the paper.

References

[1] ITER design description document. Magnet: Section 1: Engineering description, N 11 DDD 178 04-06-04 R 0.4, 2004.
[2] Zanino R, Mitchell N, Savoldi Richard L. Analysis and interpretation of the full set (2000–2002) of Tcs tests in conductor 1A of the ITER central solenoid model coil. Cryogenics 2003;43:179–97.
[3] Zanino R, Bagnasco M, Dittrich G, Fietz WH, Fillunger H, Hampshire DP, et al. Tcs tests and performance assessment of the ITER toroidal field model coil (Phase II). IEEE Trans Appl Supercond 2004;14:1519–22.
[4] Hamada K, Takahashi Y, Matsui K, Kato T, Okuno K. Effect of electromagnetic force on the pressure drop and coupling loss of a cable-in-conduit conductor. Cryogenics 2004;44:45–52.
[5] Zanino R, Gung CY, Hamada K, Savoldi L. Pressure drop analysis in the CS insert coil. Adv Cryo Eng 2002;47:364–71.
[6] Zanino R, Bruzzone P, Savoldi Richard L. A critical assessment of pressure-drop design criteria for the conductors of the ITER magnets. Adv Cryo Eng, in press.
[7] Arp V. Thermodynamics of single-phase one-dimensional fluid flow. Cryogenics 1975;15:285–9.
[8] Marinucci C. A numerical model for the analysis of stability and quench characteristics of forced-flow cooled superconductors. Cryogenics 1983;23:579–86.
[9] Bottura L. A numerical model for the simulation of quench in the ITER magnets. J Comput Phys 1996;125:26–41.
[10] Zanino R, DePalo S, Bottura L. A two-fluid code for the thermohydraulic transient analysis of CICC superconducting magnets. J Fus Energy 1995;14:25–40.
[11] Bottura L, Rosso C, Breschi M. A general model for thermal, hydraulic and electric analysis of superconducting cables. Cryogenics 2000;40:617–26.
[12] Mitchell N. Modelling of non-uniform current diffusion coupled with thermohydraulic effects in superconducting cables. Cryogenics 2000; 40:637–53.
[13] Savoldi L, Zanino R. M&M: Multi-conductor Mithrandir code for the simulation of thermal-hydraulic transients in superconducting magnets. Cryogenics 2000;40:179–89.
[14] Long A. Transverse heat transfer in a cable-in-conduit conductor with central cooling channel. Master of Science in Mechanical Engineering Thesis, MIT, 1995.
[15] Colburn AP. A method of correlating forced convection heat transfer data and a comparison with fluid friction. Trans AIChe 1933;29: 174–210.
[16] Martinez A. Numerical model for helium flow in a dual-channel cable-in-conduit-conductor. In: Proceedings of the 17th International Cryogenic Engineering Conference, 1998. p. 831–4.
[17] Feng J. A quasi-2D model for helium flow in 2-channel CICC. Adv Cryo Eng 2004;49:807–14.
[18] Inaguchi T, Hasegawa M, Koizumi N, Isono T, Hamada K, Sugimoto M, et al. Quench analysis of an ITER 13 T-40 kA Nb_3Sn coil (CS insert). Cryogenics 2004;44:121–30.
[19] Zanino R, Santagati P, Savoldi L, Martinez A, Nicollet S. Friction factor correlation with application to the central cooling channel of cable-in-conduit super-conductors for fusion magnets. IEEE Trans Appl Supercond 2000;10:1066–9.
[20] Zanino R, Savoldi L, Tessarin F, Bottura L. Effects of bundle/hole coupling parameters in the two-fluid thermal-hydraulic analysis of quench propagation in two-channel cable-in-conduit conductors. IEEE Trans Appl Supercond 1999;9:608–11.
[21] Shatil N, Zhelamskij M, Anghel A, Vecsey G, Takahashi Y, Hamada K. The first experimental observation of the He mass exchange between cable space and central channel in CICC obtained by SHF method during QUELL. In: Proceedings of the 20th Symposium on Fusion Technology, 1998. p. 715–8.
[22] Lue JW, Miller JR, Lottin JC. Pressure drop measurement on forced flow cable conductors. IEEE Trans Mag 1979;15:53–5.
[23] Katheder H. Optimum thermohydraulic operation regime for cable-in-conduit superconductors. Cryogenics 1994;34:595–8 [ICEC supplement];
Katheder H. A general formula for calculation of the friction factor for cable in conduit conductors. NET Report N/R/0821/26/A, 1993.
[24] Nicollet S, Cloez H, Duchateau JL, Serries JP. Hydraulics of the ITER toroidal field model coil cable-in-conduit conductors. In: Proceedings of the 20th Symposium on Fusion Technology, 1998. p. 715–8.
[25] Bruzzone P. Pressure drop and helium inlet in the ITER CS1 conductor. Fus Eng Des 2001;58–59:211–5.
[26] Marinucci C, Bruzzone P, della Corte A, Savoldi Richard L, Zanino R. Pressure drop of the ITER PFI cable-in-conduit conductor. IEEE Trans Appl Supercond 2005;15:1383–6.
[27] Bai H. HT-7U CICC pressure loss test. Private communication, 2001.

[28] Weng PD, Chen ZM, Wu Y, Tan YF. Quench current measurement and performance evaluation of the EAST toroidal field coils. Fus Eng Des 2005;75–79:143–8;
Wu Y. A calculation of steady pressure drop and an analysis of HT-7U CICC. Plasma Sci Technol 2002;4:1395–8.
[29] Kim K, Park HK, Park KR, Lim BS, Lee SI, Chu Y, et al. Status of the KSTAR superconducting magnet system development. Nucl Fusion 2005;45:783–9.
[30] Risse K. Overview and status of the W7-X coils. Presented at the ITER conductor meeting. Switzerland: Muerren; January 2005;
Maix RK. Some remarks on layout, fabrication and behavior of the superconductor for the W7-X coils. Presented at the ITER conductor meeting. Switzerland: Muerren; January 2005.
[31] Nield DA, Bejan A. Convection in porous media. New York: Springer; 1999.
[32] Hamada K, Takahashi Y, Koizumi N, Tsuji H, Anghel A, Blau B, et al. Thermal and hydraulic measurement in the ITER QUELL experiments. Adv Cryo Eng 1998;43:197–204.
[33] Nicollet S, Duchateau JL, Fillunger H, Martinez A, Parodi S. Dual Channel cable in conduit thermohydraulics: influence of some design parameters. IEEE Trans Appl Supercond 2000;10:1102–5.
[34] Hamada K, Kato T, Kawano K, Hara E, Ando T, Tsuji H, et al. Experimental results of pressure drop measurement in ITER CS model coil tests. Adv Cryo Eng 2002;47:407–14.
[35] Nicollet S, Duchateau JL, Fillunger H, Heller R, Maix R, Savoldi L, et al. Hydraulic resistance of the ITER toroidal field model coil dual channel cable-in-conduit conductor pancake. In: Proceedings of the 19th International Cryogenic Engineering Conference, 2002. p. 161–4.
[36] Zanino R, Bagnasco M, Fillunger H, Heller R, Savoldi Richard L, Suesser M, et al. Thermal-hydraulic issues in the ITER toroidal field model coil (TFMC) test and analysis. Adv Cryo Eng 2004;49:685–92.
[37] Ricci M. Private communication, 2005.
[38] Bruzzone P. Private communication, 2005.
[39] Marinucci C. Pressure drop of the ITER PFIS cable-in-conduit conductor. Second measurement campaign: Hole open 2005. Report CRPP/SC/2005/CM-01 2005.
[40] Zanino R, Savoldi Richard L. Task TW1-TMC CODES design and interpretation codes. Del. 1a. Part 1: Investigation on flow characteristics. Analysis of pressure drop tests in OTHELLO. April 2005 (unpublished).
[41] Ito H. Friction factors for turbulent flow in curved pipes. Trans ASME Series D (J Basic Eng) 1959;81:123–34.
[42] Bottura L. Modelling stability in superconducting cables. Phisica C 1998;310:316–26.
[43] Stekly ZJJ, Zar JL. Stable superconducting coils. IEEE Trans Nucl Sci 1965;12:367.
[44] Koizumi N, Takahashi Y, Tsuji H. Numerical model using an implicit finite difference algorithm for stability simulation of a cable-in-conduit superconductor. Cryogenics 1996;36:649–59.
[45] Zanino R, Savoldi L. Tests and modeling of heat generation and heat exchange in the full size joint sample. In: Proceedings of the 18th International Cryogenic Engineering Conference, 2000. p. 363–6.
[46] Savoldi L, Salpietro E, Zanino R. Inductively driven transients in the CS Insert Coil (II): quench tests and analysis. Adv Cryo Eng 2002;47:423–30.
[47] Handley D, Heggs PJ. Momentum and heat transfer mechanisms in regular shaped packings. Trans Inst Chem Engrs 1968;46:T251–64.
[48] Van Sciver SW. Helium cryogenics. New York: Plenum; 1986.
[49] Takahata K, Tamura H, Mito T. Thermal contact conductance between the bundle and the conduit in cable-in-conduit conductors. IEEE Trans Appl Supercond 2004;14:1477–80.
[50] Martinez A, Turck B. Supercritical helium cooling of a cable in conduit conductor with an inner tube. CEA-DRFC-STIF Internal note P/EN/93.18, 1993;
Duchateau J-L. Cable in conduit superconductors. In: Seeber B, editor. Handbook of applied superconductivity. Bristol: Institute of Physics Publishing; 1998 [chapter B6].
[51] Shaji A, Freidberg JP. Analysis of heat slug propagation. In: Anghel A, Blau B, Fuchs AM, Heer B, Marinucci C, et al., editors, The quench experiment on long length (QUELL). Final report. Villigen, Naka, Cambridge, St. Petersburg, 1997. p. 128–30 [section 3.2.2].
[52] Bottura L, Bruzzone P, Marinucci C, Stepanov B. Transverse heat transfer in CICC's with Central cooling channel. Presented at the ITER Conductor Meeting, Muerren, Switzerland, January 2005;
Bottura L, Bruzzone P, Marinucci C, Stepanov B. Analytical temperature front propagation in CICCs with central cooling hole. Presented at CHATS Meeting, Netherlands: Twente University, June 2005.
[53] Duchateau JL. Heat exchange evaluation between central channel and bundle region. Steady state approach. Presented at the ITER Conductor Meeting. Switzerland: Muerren, January 2005;
Renard B, Martinez A, Duchateau JL, Tadrist L. Transient measurements of dual-channel CICC heat transfer coefficients on a full-size ITER conductor. Presented at CHATS Meeting. Netherlands: Twente University, June 2005.
[54] Zanino R, Decool P, Savoldi Richard L. Status of the analysis of HECOL transient heat transfer tests. Presented at the ITER conductor meeting. Switzerland: Muerren, January 2005.
[55] Ciazynski D. Tests of PF-FSJS in SULTAN: Thermohydraulics and calibration. CRPP Workshop on 15 months of NbTi CICC results in SULTAN. Switzerland: Gstaad, 2003.
[56] Zanino R, Bruzzone P, Ciazynski D, Ciotti M, Gislon P, Nicollet S, et al. Analysis of thermal-hydraulic gravity/buoyancy effects in the testing of the ITER poloidal field full size joint sample (PF-FSJS). Adv Cryo Eng 2004;49:544–51.
[57] Bruzzone P, Stepanov B, Zanino R, Savoldi Richard L. Results of buoyancy-gravity effects in ITER cable-in-conduit conductor with dual channel. Adv Cryo Eng, in press.
[58] Duchateau JL, Renard B. Possible thermosiphon effect between bundle and hole regions in the ITER TF conductor along the TF coil inner leg. CEA Report AIM/NTT-2004.006, 2004.
[59] Pasler V. Numerical investigation of buoyancy effects in vertical ITER-TF-CICC parts at normal operating conditions. Presented at CHATS meeting. Netherlands: Twente University, June 2005.
[60] Savoldi L, Michael P, Zanino R. Tests and simulation of thermal-hydraulic transients in the US prototype joint sample. Int J Mod Phys B 2000;14:3183–8.
[61] Nicollet S, Cloez H, Decool P, Duchateau JL, Martinez A, Tena M, et al. Experimental investigation to determine the heat transfer coefficient between annular area and the central channel of ITER-FEAT conductors as an input to codes development. CEA Report AIM/NTT-2004.017 2004.
[62] Bruzzone P, Fuchs AM, Vecsey G, Zapretilina E. Test results for the high field conductor of the ITER Central Solenoid Model Coil. Adv Cryo Eng 2000;45:729–36.
[63] Zanino R, Savoldi L. Status and perspectives of thermal-hydraulic analysis of superconducting magnets for nuclear fusion applications. IAEA-CSP-8/C CD-ROM proceedings. Paper FTP2/01, IAEA, Vienna, May 2001.
[64] Zanino R, Giors S, Mondino R. CFD modeling of ITER cable-in-conduit super-conductors. Part I: Friction in the central channel. Adv Cryo Eng 2006.
[65] Ferziger JH, Peric M. Computational methods for fluid dynamics. Berlin: Springer; 1996.
[66] Wilcox DC. Turbulence modeling for CFD. La Canada (CA): DCW Industries; 1993.
[67] Zanino R, Bagnasco M, Baker W, Bellina F, Bruzzone P, della Corte A, et al. Implications of NbTi short-sample test results and analysis for the ITER Poloidal Field Conductor Insert (PFCI). IEEE Trans Appl Supercond, in press.